Tailoring 3D Speckle Statistics

SeungYun Han,[1] Nicholas Bender,[2] and Hui Cao[1,*]
[1]Department of Applied Physics, Yale University, New Haven, Connecticut 06520, USA
[2]School of Applied and Engineering Physics, Cornell University, Ithaca, New York 14850, USA

(Received 29 July 2022; accepted 26 January 2023; published 3 March 2023)

We experimentally generate three-dimensional speckles with customized intensity statistics. By appropriately modulating the phase front of a laser beam, the far-field speckles can maintain a desired intensity probability density function upon axial propagation: while evolving into different spatial patterns. We also demonstrate how to design speckle patterns that obtain distinct tailored intensity statistics on multiple designated axial planes. The ability to design 3D speckle statistics opens many possibilities: three-dimensional imaging and sensing, optical trapping, and manipulation.

DOI: 10.1103/PhysRevLett.130.093802

Speckles occur in various waves: electromagnetic, acoustic, and matter. They are produced by interference between numerous partial waves with uncorrelated phases. Characterized by a random granular pattern of diffraction-limited grains, fully developed speckles typically satisfy Rayleigh statistics [1,2]. By introducing high-order correlations into the interfering partial waves, fully developed speckle patterns can be created, possessing circular non-Gaussian statistics on a single plane, i.e., a customized intensity probability density function (PDF) and/or long-range spatial correlations [3–7]. However, the high-order correlations erode away with axial propagation, and the customized speckles revert back to Rayleigh statistics. Whether it is possible to create axially varying volumetric speckles with tailored statistics remains an open question. The major challenge to creating volumetric non-Rayleigh speckles is controlling the high-order correlations of the partial waves over an extended axial range: overcoming the field evolution accompanying free-space propagation.

The recent interest in customizing statistical properties of speckle patterns [3–16] stems, in large part, from their numerous practical applications. Optical speckles have been widely employed in structured-illumination imaging [17–35], and sensing applications [36–39]. While Rayleigh speckles are commonly used, super-Rayleigh and other types of customized speckles can improve image resolution, visibility, and signal to noise ratio [40–44]. Specially designing the intensity statistics of speckles used in parallelized nonlinear pattern-illumination microscopy enables a 3 times higher spatial resolution than provided by the optical diffraction limit [7]. However, improving the axial resolution—via speckle customization—was not explored. Tailoring the statistics of speckles along the axial direction can provide a better axial resolution in three-dimensional (3D) imaging [29]. Moreover, the optical potentials created by 3D customized speckles can provide an effective platform for studying 3D transport and localization of cold atoms [45–49] and active media in random potentials [50,51]. Tailored speckles may also be used to manipulate, sort, and order microparticles in three dimensions [52–55].

In this Letter, we experimentally demonstrate a method to customize the intensity statistics of 3D speckles. Specifically, we control the intensity probability density functions of speckle patterns on multiple axial planes. This is accomplished by appropriately manipulating the phase front of a laser beam, with a spatial light modulator. We can tailor the far-field speckles to maintain a desired intensity PDF, while propagating axially and evolving into distinct patterns. When this occurs, the high-order correlations encoded into the (spatial) Fourier fields are preserved over an extended axial range. We can also create speckles with different intensity PDFs on multiple planes, demonstrating that distinct high-order correlations can be encoded at varying axial locations. This unprecedented control over 3D light statistics opens the door for customizing volumetric speckle fields in various applications.

Our experimental setup consists of a laser (wavelength $\lambda = 638$ nm), a phase-only spatial light modulator (SLM), an optical lens (focal length $= 20$ cm), and a CCD camera [6]. The SLM is placed at the front focal plane of the lens, and is fully illuminated by the linearly polarized laser beam. The light reflected off the SLM is collected by the lens, projected onto a CCD camera, which is mounted on a motorized translation stage to move axially and record speckle patterns on different transverse planes. In the SLM, a phase-modulation region with 512×512 pixels is divided to 32×32 macropixels (16×16 pixels binned to a single macropixel). The camera has 199×199 pixels to record ~770 speckle grains. When a random phase pattern is displayed on the SLM, a Rayleigh speckle pattern is generated at the back focal plane of the lens ($z = 0$). It evolves upon axial propagation and becomes decorrelated. We compute the axial correlation function of the speckle's intensity, and define its full-width-at-half-maximum as the

axial decorrelation length $R_l = 9.3$ cm. To a good approximation, the field incident on the camera at the back focal plane of the lens ($z = 0$) is a Fourier transform of the field reflected off the SLM. To be more precise and general, we measure the field-transmission matrix between them, to account for experimental artifacts such as lens aberrations and optical misalignment [56].

Two examples of experimentally measured 3D speckles, customized to have different intensity statistics, are presented in Fig. 1. An example of volumetric speckles with an intensity PDF tailored to be flat, $P(I/\langle I\rangle) = 0.5$ over a predefined range of intensity values $0 \le I/\langle I\rangle \le 2$, is shown in Fig. 1(a), where $\langle I\rangle$ denotes the mean intensity. The 2D speckle pattern in the Fourier plane ($z/R_l = 0$) axially evolves and eventually decorrelates with its original spatial profile at $z/R_l = 1$ [56]. Even though the speckle pattern decorrelates, the intensity PDF remains constant over two axial-decorrelation lengths $0 \le z/R_l \le 2$. Similarly, Fig. 1(b) is an example of volumetric speckles with a unimodal intensity PDF. Again, the PDF is axially invariant despite the axial decorrelation of the speckles. The customized intensity PDF, therefore, dictates volumetric statistics of the speckles.

The major challenge we combat when customizing the statistics of 3D speckles, like those shown in Fig. 1, is the fact that the 2D fields on different axial planes are related. Specifically, the field profile on one axial plane will determine the fields on all subsequent propagation distances along z.

The algorithm we developed to overcome the propagation-relation challenge is illustrated in Fig. 2, and entails the following steps. When generating speckles with intensity PDFs tailored over a volume extending across two axial-decorrelation lengths ($0 \le z \le 2R_l$), we optimize the speckle patterns on 11 transverse planes, separated by $\Delta z = 0.2R_l$. With such axial spacing, the speckles only change slightly between adjacent planes. For a given phase pattern displayed on the SLM, the corresponding speckle patterns on each of the 11 planes can be numerically calculated via the measured transmission matrix and a convolution with the Fresnel propagation kernel. In order to tailor the intensity statistics of the speckles across these planes, we start with Rayleigh speckles—generated by a random phase pattern on the SLM—and iteratively apply local-intensity transformations to the spatial intensity-patterns of each plane [56]. More specifically, transforming an intensity pattern $I(r)$ of PDF $P(I)$ to a new one $\tilde{I}(r)$ with target PDF $F(\tilde{I})$ is realized with the mapping $\tilde{I} = f(I)$ obtained from $\int_0^I P(I')dI' = \int_0^{\tilde{I}} F(\tilde{I}')d\tilde{I}'$. The transformed field amplitude is then combined with the original phase. Such process breaks the propagation relation between the 11 planes. This can be partially recovered, however, by a subsequent procedure of "propagation averaging." To do so we select one plane, for example, the first plane, and numerically propagate the other 10 planes to the chosen plane, and average the corresponding fields on that plane (11 in total). The averaged field is converted to a SLM plane with the measured transmission matrix. The resulting phase-modulation pattern is kept, and the amplitude modulation is removed. This process is then iteratively repeated with the new phase-modulation pattern, until the fields on all planes satisfy the propagation relation and the target

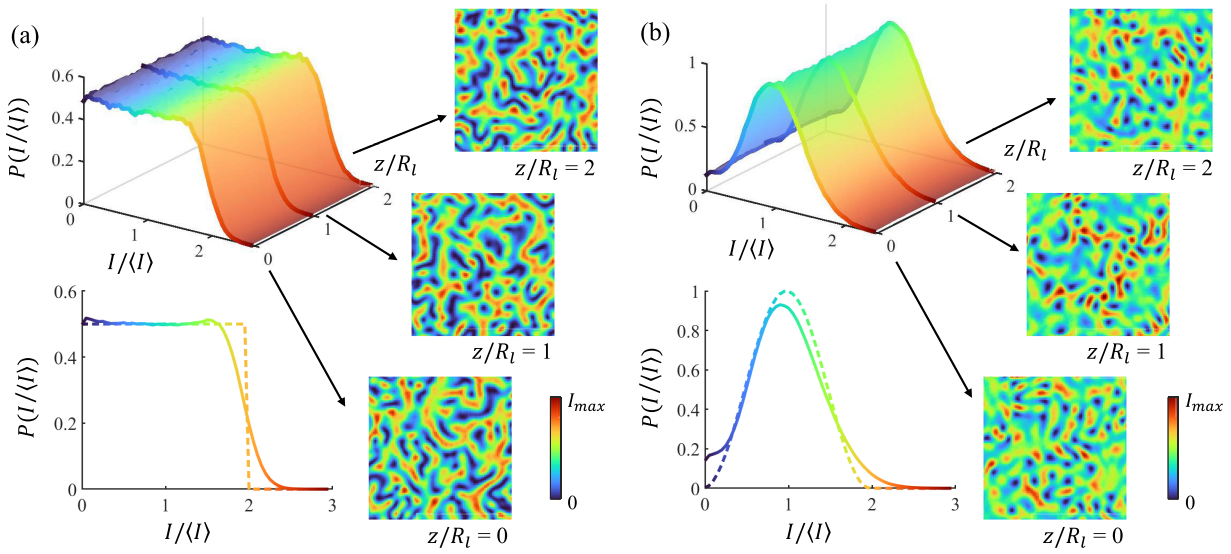

FIG. 1. Experimental realizations of volumetric speckles with customized intensity PDFs. $P(I/\langle I\rangle)$ is uniform within the range $0 \le I/\langle I\rangle \le 2$ in (a), and peaked at $I/\langle I\rangle = 1$ in (b). Top left graph in (a),(b) shows axial-invariant intensity PDF, bottom left graph is the intensity PDF obtained within two axial-decorrelation lengths. Speckle patterns evolve axially as shown in the right for axial locations $z/R_l = 0$, 1, 2. The axial-decorrelation length $R_l = 9.3$ cm. Each speckle image corresponds to 90×90 camera pixels (504×504 μm^2). Intensity PDFs are obtained by averaging over 30 speckle realizations.

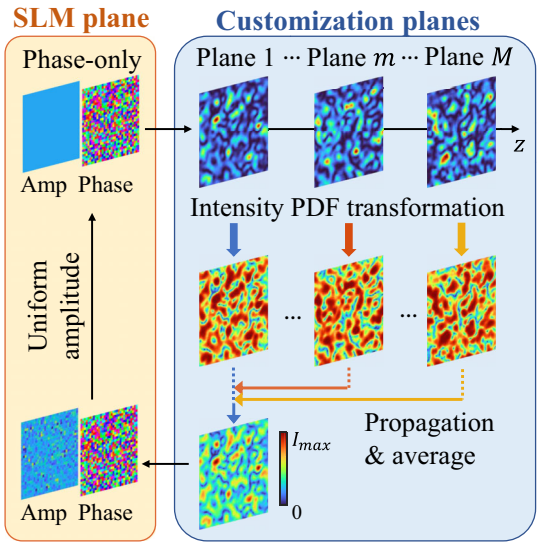

FIG. 2. Numerical algorithm for tailoring 3D speckle statistics. A schematic illustration of customizing the speckle intensity PDFs across M axial planes. Starting with Rayleigh speckles generated by a random phase pattern on the SLM, a local intensity transformation is applied independently to each plane to obtain the target PDF. Modified fields in all planes are propagated to one plane and averaged. The averaged field is projected to the SLM plane and then the amplitude is set uniform. The new phase pattern on SLM is used as the input of the next round. This process is iterated until the fields in all planes satisfy the propagation relation and the target intensity PDF.

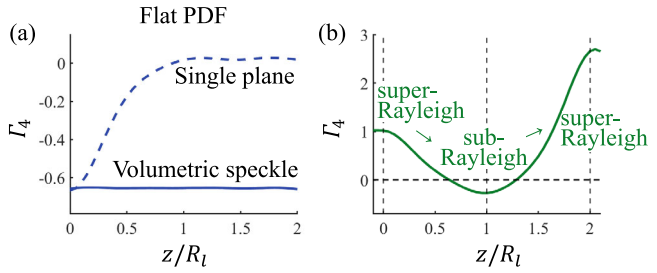

FIG. 3. High-order correlations of Fourier fields. (a) $\Gamma_4(z) = C^2(z) - 1$ for volumetric speckles in Fig. 1(a) with flat intensity PDF (blue solid curve) stays nearly constant with z. For comparison, $\Gamma_4(z)$ returns to 0 (blue dashed curve) within one axial-decorrelation length R_l, when the flat intensity PDF is designated only to a single plane ($z = 0$). (b) Axial variation of Γ_4 when speckle intensity PDF transforms from super-Rayleigh at $z/R_l = 0$ to sub-Rayleigh at $z/R_l = 1$ and back to super-Rayleigh at $z/R_l = 2$ in Fig. 4(b). Γ_4 changes sign twice, since its value is positive for super-Rayleigh and negative for sub-Rayleigh. Γ_4 values in (a),(b) are obtained by averaging over 30 speckle realizations.

intensity PDF. Typically, this process converges by 1000 iterations, and the final phase-modulation pattern is displayed on the SLM. Repetition of this procedure with different initial random phase patterns on the SLM creates a set of independent 3D speckle patterns that possesses the same intensity statistics. Note that experimentally (Fig. 1) we measure speckle patterns on 41 planes with axial spacing of $0.05R_l$, much smaller than the spacing of 11 planes in the optimization and the intensity statistics remain constant. This confirms that the chosen spacing of $0.2R_l$ is sufficient for "volumetric" control of the speckles' statistics. We verify that the speckles generated with this technique are fully developed [6], by calculating the joint complex-field PDF [56]. Its circularity reveals that the speckle fields have an isotropic phase distribution over $[0, 2\pi)$, thus they are fully developed.

Through customization, our algorithm encodes high-order correlations into the speckle fields. This can be seen via the speckle intensity contrast. The intensity contrast C of the customized speckles is determined by the target PDF, and deviates from 1 for Rayleigh speckles. As derived in Ref. [3], $C^2(z) \simeq 1 + \Gamma_4(z)$, and

$$\Gamma_4(z) \propto \sum \tilde{E}(\mathbf{k}_1, z)\tilde{E}(\mathbf{k}_2, z)\tilde{E}(\mathbf{k}_3, z)\tilde{E}(\mathbf{k}_1 + \mathbf{k}_2 - \mathbf{k}_3, z), \quad (1)$$

where $\tilde{E}(\mathbf{k}, z)$ is transverse Fourier transform of speckle field $E(\mathbf{r}, z)$, $\mathbf{k}$ is the transverse wave vector, and the summation in Eq. (1) is over $\mathbf{k}_1$, $\mathbf{k}_2$, and $\mathbf{k}_3$ with the constraint $\mathbf{k}_1 \neq \mathbf{k}_2 \neq \mathbf{k}_3$. Thus, non-Rayleigh speckle statistics ($C \neq 1$) at $z = 0$ result from high-order correlations Γ_4 encoded into the Fourier fields $\tilde{E}(\mathbf{k}, z)$. If only the speckle statistics on one plane are customized, Γ_4 will vanish upon axial propagation, and C will return to 1 within one axial-decorrelation length [dashed line in Fig. 3(a)]. The axial propagation corresponds to multiplying the optimized Fourier field profile by the Fresnel propagation kernel, which tends to destroy the high-order correlations. For volumetric customized speckles, the high-order correlations between the Fourier fields $\tilde{E}(\mathbf{k}, z)$ are preserved over extended axial propagation. This is shown by the solid line in Fig. 3(a), where Γ_4 stays at a nonzero, constant value across two axial-decorrelation lengths.

Until now, we have focused on generating speckles with a uniform volumetric PDF. Nothing prevents us, however, from using the same technique for a different goal: generating speckles with axially varying PDFs. Here, we demonstrate that our method is also able to create speckles with distinct statistics on different axial planes. As an example, we select three planes separated by one axial-decorrelation length, $z/R_l = 0, 1, 2$. Shown in Fig. 4(a), the speckle intensity PDFs for the three planes are designated to be unimodal, flat, and bimodal. We apply the same algorithm for volumetric speckles to the three planes, and obtain the SLM phase pattern. Experimentally we record the speckle patterns over the axial range of $0 \leq z/R_l \leq 2$ and obtain the intensity PDF of each plane. Figure 4(a) shows the measured PDF evolving from unimodal at $z = 0$ to flat at $z/R_l = 1$, and to bimodal at $z/R_l = 2$. Thus, the

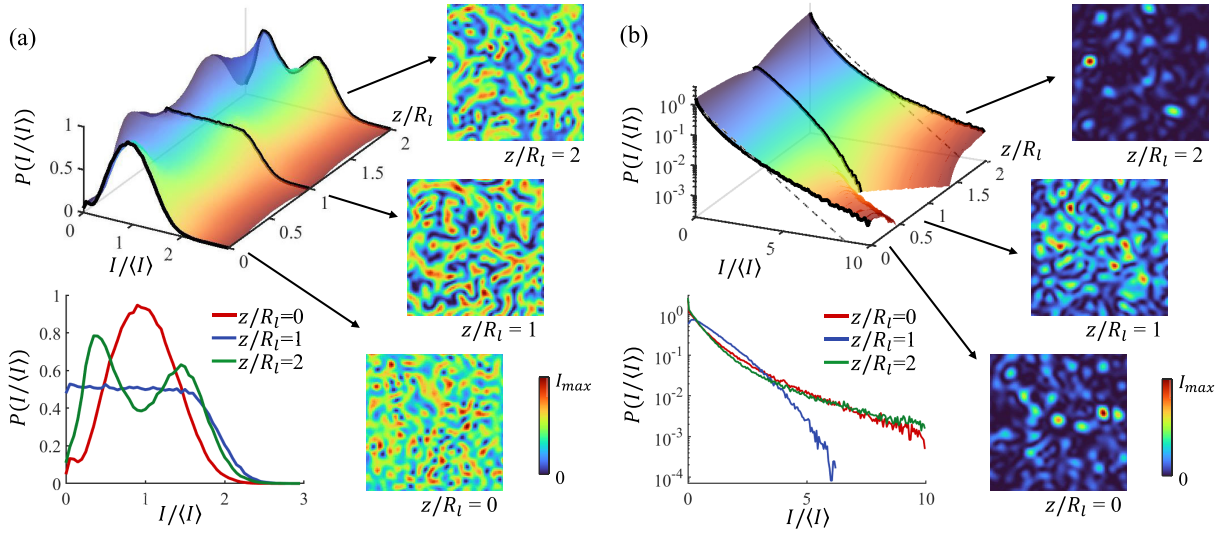

FIG. 4. Experimental realizations of distinct speckle statistics on three planes. Speckle intensity PDFs at three axial planes, $z/R_l = 0$, 1, 2, are unimodal, flat, bimodal in (a); super-Rayleigh, sub-Rayleigh, super-Rayleigh in (b). Top left graph in (a),(b) shows an axially evolving intensity PDF, bottom left graph is the intensity PDF at $z/R_l = 0$, 1, 2. Speckle patterns at the three designated planes are shown on the right. All parameters are identical to those in Fig. 1.

intensity PDFs on different planes can be tailored simultaneously and independently for axial-evolving speckle patterns. We have found that the separations between the designated planes can vary, so long as they all exceed a minimum distance ($\sim 0.2R_l$): otherwise, the speckles do not have enough propagation distance to transition between PDFs. A second example is given in Fig. 4(b), where the speckles evolve from super-Rayleigh at $z = 0$ to sub-Rayleigh at $z/R_l = 1$ and then back to super-Rayleigh at $z/R_l = 2$. Here, the super and sub-Rayleigh refer to intensity PDFs that decay faster or slower than a Rayleigh PDF [3]. Γ_4 is positive for super-Rayleigh, and negative for sub-Rayleigh. Figure 3(b) shows the axial variation of Γ_4 over two axial-decorrelation lengths. Starting from a positive value at $z/R_l = 0$, it drops and crosses zero to reach a negative value at $z/R_l = 1$, then it rises to cross zero and become positive again at $z/R_l = 2$. Therefore, a single SLM phase pattern can encode distinct high-order correlations among the Fourier components of speckle fields at varying axial locations.

Previously non-Rayleigh speckle patterns were made axially invariant by imposing a ring-shaped amplitude mask to the SLM phase pattern [16], in analogy to the generation of diffraction-free beams [59]. Such methods cannot create axially evolving speckle patterns with non-Rayleigh statistics, while our method can. Moreover, our method does not require amplitude modulation, thus minimizing power loss. No current theory predicts, or even hints at, the possibility of tailoring 3D speckle statistics with a single phase-modulation pattern: as we demonstrate here using an iterative algorithm. Without numerical optimization, it would be much more challenging to design volumetric speckle patterns *a priori*, because the far-field speckle intensities are related to the near-field phase pattern by transcendental equations, which cannot be solved analytically.

In conclusion, we have developed an efficient method for customizing 3D speckle intensity statistics and experimentally demonstrated it using a phase-only SLM. Our method of customizing 3D speckle statistics is compatible with a broad range of experimental setups. It opens up opportunities for fundamental studies on transport and localization of cold atoms and colloidal particles in 3D optical potentials created by laser speckles with tailored statistics. For example, it has been shown that a lack of symmetry in a speckle intensity PDF $P(I)$, with respect to the mean intensity $\langle I\rangle$, leads to an asymmetric distribution of the on-site potential; modifying the mobility edge of cold atoms [47]. Our method can be used to generate 3D speckles with symmetric $P(I)$ and further tune the asymmetry of $P(I)$ to study its effect on the mobility edge. Additionally, it may be possible to extend our method to tailor the spatial intensity correlations of 3D speckles, which will enable a systematic study on how the anisotropy of disordered potentials affects the mobility edge [48].

Our work also paves the way for new directions in applied research such as 3D speckle-based imaging, holography sensing, optical trapping and manipulation. For instance, in dynamic speckle illumination microscopy and HiLo microscopy [17,60], the speckle contrast is an important factor that determines the axial sectioning ability. Our numerical simulation shows that an axial evolution from super-Rayleigh to sub-Rayleigh speckles leads to a varying intensity contrast that can significantly improve the axial resolution [56]. While the axial range is set to two axial-decorrelation lengths in the demonstrations above,

it is possible to tailor the speckle statistics over a wider range. We numerically calculate the number of SLM pixels M_s needed to customize speckle intensity PDFs on M_p planes (separated by R_l), and find M_p increases linearly with M_s [56]. Therefore, the axial range of speckle customization can be extended well beyond $2R_l$ as long as the SLM has sufficient degrees of control.

This work is supported by the U.S. Office of Naval Research (ONR) under Grant No. N00014-221-1-2026.

*hui.cao@yale.edu

[1] J. W. Goodman, *Speckle Phenomena in Optics: Theory and Applications* (Roberts and Company Publishers, Greenwood Village (Colorado), 2007)
[2] J. C. Dainty, *Laser Speckle and Related Phenomena* (Springer Science & Business Media, New York, 2013), Vol. 9.
[3] Y. Bromberg and H. Cao, Generating Non-Rayleigh Speckles with Tailored Intensity Statistics, Phys. Rev. Lett. **112**, 213904 (2014).
[4] N. Bender, H. Yılmaz, Y. Bromberg, and H. Cao, Customizing speckle intensity statistics, Optica **5**, 595 (2018).
[5] N. Bender, H. Yılmaz, Y. Bromberg, and H. Cao, Introducing non-local correlations into laser speckles, Opt. Express **27**, 6057 (2019).
[6] N. Bender, H. Yılmaz, Y. Bromberg, and H. Cao, Creating and controlling complex light, APL Photonics **4**, 110806 (2019).
[7] N. Bender, M. Sun, H. Yılmaz, J. Bewersdorf, and H. Cao, Circumventing the optical diffraction limit with customized speckles, Optica **8**, 122 (2021).
[8] A. Dogariu and R. Carminati, Electromagnetic field correlations in three-dimensional speckles, Phys. Rep. **559**, 1 (2015).
[9] R. Fischer, I. Vidal, D. Gilboa, R. R. Correia, A. C. Ribeiro-Teixeira, S. D. Prado, J. Hickman, and Y. Silberberg, Light with Tunable Non-Markovian Phase Imprint, Phys. Rev. Lett. **115**, 073901 (2015).
[10] J. P. Amaral, E. J. S. Fonseca, and A. J. Jesus-Silva, Tailoring speckles with weibull intensity statistics, Phys. Rev. A **92**, 063851 (2015).
[11] H. E. Kondakci, A. Szameit, A. F. Abouraddy, D. N. Christodoulides, and B. E. Saleh, Sub-thermal to super-thermal light statistics from a disordered lattice via deterministic control of excitation symmetry, Optica **3**, 477 (2016).
[12] X. Li, Y. Tai, H. Li, J. Wang, H. Wang, and Z. Nie, Generation of a super-rayleigh speckle field via a spatial light modulator, Appl. Phys. B **122**, 1 (2016).
[13] D. Di Battista, D. Ancora, M. Leonetti, and G. Zacharakis, Tailoring non-diffractive beams from amorphous light speckles, Appl. Phys. Lett. **109**, 121110 (2016).
[14] D. Di Battista, D. Ancora, G. Zacharakis, G. Ruocco, and M. Leonetti, Hyperuniformity in amorphous speckle patterns, Opt. Express **26**, 15594 (2018).
[15] L. Devaud, B. Rauer, J. Melchard, M. Kühmayer, S. Rotter, and S. Gigan, Speckle Engineering Through Singular Value Decomposition of the Transmission Matrix, Phys. Rev. Lett. **127**, 093903 (2021).
[16] R. Liu, B. Qing, S. Zhao, P. Zhang, H. Gao, S. Chen, and F. Li, Generation of Non-Rayleigh Nondiffracting Speckles, Phys. Rev. Lett. **127**, 180601 (2021).
[17] C. Ventalon and J. Mertz, Quasi-confocal fluorescence sectioning with dynamic speckle illumination, Opt. Lett. **30**, 3350 (2005).
[18] D. Lim, K. K. Chu, and J. Mertz, Wide-field fluorescence sectioning with hybrid speckle and uniform-illumination microscopy, Opt. Lett. **33**, 1819 (2008).
[19] D. Lim, T. N. Ford, K. K. Chu, and J. Metz, Optically sectioned in vivo imaging with speckle illumination hilo microscopy, J. Biomed. Opt. **16**, 016014 (2011).
[20] S. Bernet, W. Harm, A. Jesacher, and M. Ritsch-Marte, Lensless digital holography with diffuse illumination through a pseudo-random phase mask, Opt. Express **19**, 25113 (2011).
[21] E. Mudry, K. Belkebir, J. Girard, J. Savatier, E. Le Moal, C. Nicoletti, M. Allain, and A. Sentenac, Structured illumination microscopy using unknown speckle patterns, Nat. Photonics **6**, 312 (2012).
[22] J. Min, J. Jang, D. Keum, S.-W. Ryu, C. Choi, K.-H. Jeong, and J. C. Ye, Fluorescent microscopy beyond diffraction limits using speckle illumination and joint support recovery, Sci. Rep. **3**, 2075 (2013).
[23] E.-F. Zhang, W.-T. Liu, and P.-X. Chen, Ghost imaging with non-negative exponential speckle patterns, J. Opt. **17**, 085602 (2015).
[24] H. Yilmaz, E. G. van Putten, J. Bertolotti, A. Lagendijk, W. L. Vos, and A. P. Mosk, Speckle correlation resolution enhancement of wide-field fluorescence imaging, Optica **2**, 424 (2015).
[25] D. Phillips, R. He, Q. Chen, G. Gibson, and M. Padgett, Non-diffractive computational ghost imaging, Opt. Express **24**, 14172 (2016).
[26] T. Chaigne, J. Gateau, M. Allain, O. Katz, S. Gigan, A. Sentenac, and E. Bossy, Super-resolution photoacoustic fluctuation imaging with multiple speckle illumination, Optica **3**, 54 (2016).
[27] A. K. Singh, D. N. Naik, G. Pedrini, M. Takeda, and W. Osten, Exploiting scattering media for exploring 3d objects, Light Sci. Appl. **6**, e16219 (2017).
[28] A. Vigoren and J. M. Zavislan, Optical sectioning enhancement using higher-order moment signals in random speckle-structured illumination microscopy, J. Opt. Soc. Am. A **35**, 474 (2018).
[29] M. Pascucci, S. Ganesan, A. Tripathi, O. Katz, V. Emiliani, and M. Guillon, Compressive three-dimensional super-resolution microscopy with speckle-saturated fluorescence excitation, Nat. Commun. **10**, 1327 (2019).
[30] L.-H. Yeh, S. Chowdhury, N. A. Repina, and L. Waller, Speckle-structured illumination for 3d phase and fluorescence computational microscopy, Biomed. Opt. Express **10**, 3635 (2019).
[31] H. Zhang, S. Jiang, J. Liao, J. Deng, J. Liu, Y. Zhang, and G. Zheng, Near-field fourier ptychography: Super-resolution phase retrieval via speckle illumination, Opt. Express **27**, 7498 (2019).
[32] Y. Baek, K. Lee, J. Oh, and Y. Park, Speckle-correlation scattering matrix approaches for imaging and sensing through turbidity, Sensors **20**, 3147 (2020).

[33] S. Liu, Z. Liu, C. Hu, E. Li, X. Shen, and S. Han, Spectral ghost imaging camera with super-rayleigh modulator, Opt. Commun. **472**, 126017 (2020).
[34] X. Nie, F. Yang, X. Liu, X. Zhao, R. Nessler, T. Peng, M. S. Zubairy, and M. O. Scully, Noise-robust computational ghost imaging with pink noise speckle patterns, Phys. Rev. A **104**, 013513 (2021).
[35] Y. Choi, M. Kim, C. Park, J. Park, Y. Park, and Y.-H. Cho, Wide-field super-resolution optical fluctuation imaging through dynamic near-field speckle illumination, Nano Lett. **22**, 2194 (2022).
[36] A. Anand, G. Pedrini, W. Osten, and P. Almoro, Wavefront sensing with random amplitude mask and phase retrieval, Opt. Lett. **32**, 1584 (2007).
[37] K. Kim, H. Yu, J. Koh, J. H. Shin, W. Lee, and Y. Park, Remote sensing of pressure inside deformable microchannels using light scattering in scotch tape, Opt. Lett. **41**, 1837 (2016).
[38] P. Berto, H. Rigneault, and M. Guillon, Wavefront sensing with a thin diffuser, Opt. Lett. **42**, 5117 (2017).
[39] Q. Luo, J. A. Patel, and K. J. Webb, Super-resolution sensing with a randomly scattering analyzer, Phys. Rev. Res. **3**, L042045 (2021).
[40] J.-E. Oh, Y.-W. Cho, G. Scarcelli, and Y.-H. Kim, Sub-rayleigh imaging via speckle illumination, Opt. Lett. **38**, 682 (2013).
[41] K. Kuplicki and K. W. C. Chan, High-order ghost imaging using non-rayleigh speckle sources, Opt. Express **24**, 26766 (2016).
[42] S. Zhang, W. Wang, R. Yu, and X. Yang, High-order correlation of non-rayleigh speckle fields and its application in super-resolution imaging, Laser Phys. **26**, 055007 (2016).
[43] P. Liu, Label-free storm principle realized by super-rayleigh speckle in photoacoustic imaging, Opt. Lett. **44**, 4642 (2019).
[44] Z. Li, X. Nie, F. Yang, X. Liu, D. Liu, X. Dong, X. Zhao, T. Peng, M. S. Zubairy, and M. O. Scully, Sub-rayleigh second-order correlation imaging using spatially distributive colored noise speckle patterns, Opt. Express **29**, 19621 (2021).
[45] S. Kondov, W. McGehee, J. Zirbel, and B. DeMarco, Three-dimensional anderson localization of ultracold matter, Science **334**, 66 (2011).
[46] F. Jendrzejewski, A. Bernard, K. Mueller, P. Cheinet, V. Josse, M. Piraud, L. Pezzé, L. Sanchez-Palencia, A. Aspect, and P. Bouyer, Three-dimensional localization of ultracold atoms in an optical disordered potential, Nat. Phys. **8**, 398 (2012).
[47] D. Delande and G. Orso, Mobility Edge for Cold Atoms in Laser Speckle Potentials, Phys. Rev. Lett. **113**, 060601 (2014).
[48] G. Semeghini, M. Landini, P. Castilho, S. Roy, G. Spagnolli, A. Trenkwalder, M. Fattori, M. Inguscio, and G. Modugno, Measurement of the mobility edge for 3d anderson localization, Nat. Phys. **11**, 554 (2015).
[49] E. Fratini and S. Pilati, Anderson localization of matter waves in quantum-chaos theory, Phys. Rev. A **91**, 061601(R) (2015).
[50] K. M. Douglass, S. Sukhov, and A. Dogariu, Superdiffusion in optically controlled active media, Nat. Photonics **6**, 834 (2012).
[51] L. Levi, Y. Krivolapov, S. Fishman, and M. Segev, Hyper-transport of light and stochastic acceleration by evolving disorder, Nat. Phys. **8**, 912 (2012).
[52] K. Dholakia and T. Čižmár, Shaping the future of manipulation, Nat. Photonics **5**, 335 (2011).
[53] G. Volpe, L. Kurz, A. Callegari, G. Volpe, and S. Gigan, Speckle optical tweezers: Micromanipulation with random light fields, Opt. Express **22**, 18159 (2014).
[54] G. Volpe, G. Volpe, and S. Gigan, Brownian motion in a speckle light field: Tunable anomalous diffusion and selective optical manipulation, Sci. Rep. **4**, 3936 (2014).
[55] A. S. Nunes, S. K. Velu, I. Kasianiuk, D. Kasyanyuk, A. Callegari, G. Volpe, M. M. T. da Gama, G. Volpe, and N. A. Araújo, Ordering of binary colloidal crystals by random potentials, Soft Matter **16**, 4267 (2020).
[56] See Supplemental Material at http://link.aps.org/supplemental/10.1103/PhysRevLett.130.093802 for a detailed description of transmission matrix measurement, customized speckle field analyses, application to dynamic speckle illumination microscopy, and degree of control in speckle customization. It includes Refs. [57,58].
[57] J. Yoon, K. Lee, J. Park, and Y. Park, Measuring optical transmission matrices by wavefront shaping, Opt. Express **23**, 10158 (2015).
[58] N. Bender, Controlling complex light propagation and statistics, Ph.D. thesis, Yale Graduate School of Arts and Sciences, 2021, https://www.eng.yale.edu/caolab/papers/Bender_Dissertation.pdf.
[59] J. Durnin, J. J. Miceli Jr, and J. H. Eberly, Diffraction-Free Beams, Phys. Rev. Lett. **58**, 1499 (1987).
[60] J. Mazzaferri, D. Kunik, J. Belisle, K. Singh, S. Lefrançois, and S. Costantino, Analyzing speckle contrast for hilo microscopy optimization, Opt. Express **19**, 14508 (2011).